Chapter 6
Design of Structures Prone to Pounding

At the design stage of adjacent buildings or bridge structures, the probability of occurrence of earthquake-induced structural pounding should be carefully analyzed. The minimum separation gap, so as to avoid collisions, is specified in the recent earthquake-resistant design codes (see, for example, ECS 1998, IS 2002; NBC 2003; IBC 2009). On the other hand, in the case when pounding can not be prevented, the assessment of the peak pounding force value expected during the time of the earthquake is important for the design purposes. Such an assessment can be conducted by the use of pounding force response spectrum (Jankowski 2005, 2006). Moreover, the potential structural damage of colliding structures under the design ground motion can be determined with the help of damage indices (Park and Ang 1985; Powell and Allahabadi 1988; Fajfar 1992; Cosenza et al. 1993; Bojórquez et al. 2010; Moustafa 2011).

6.1 Procedures in the Building Codes Related to the Minimum Seismic Gap

A number of building codes for seismic design around the world do not refer to earthquake-induced structural pounding phenomenon and do not include any comments how to prevent adjacent structures from impacts. Only the recent earthquake-resistant design codes, as well as a number of less formal regulatory guides, specify the minimum seismic gap for newly constructed buildings (Rajaram and Kumar 2012). The way to determine the minimum separation distance required to prevent seismic pounding between adjacent structures varies from regulation to regulation. The Canadian code considers the simplest approach in which the absolute sum of the peak displacements of two buildings should be calculated (see Eq. (5.1). The edition of 1997 of the Uniform Building Code (UBC 1997) and the edition of 2003 of the International Building Code (IBC 2003) suggest the formula of the square root of sum of squares (SRSS), as defined in Eq. (5.2). The quadratic combination of the maximum peak displacements has also been employed in

Eurocode 8 (ECS 1998). The edition of International Building Code published in 2009 modifies the requirement for determination the seismic gap distance, $d_{\min}$, suggesting that it should be rather calculated based on the following equation (IBC 2009):

$$d_{\min} = \frac{C_D \delta_{\max}}{I} \tag{6.1}$$

where C_D is the deflection amplification factor, which depends on the seismic force-resisting system, $\delta_{\max}$ represents the peak displacement calculated from the elastic analysis and I is the importance factor determined in accordance with the seismic use group. The same formula as given in Eq. (6.1) is also suggested to calculate the minimum separation gap in the guidelines of American Society of Civil Engineers (ASCE 2010).

A number of codes specify the minimum seismic gap using some ways which are independent from the dynamic characteristics of structures. The edition of Taiwan code is a good example of such a situation since the required minimum gap to avoid pounding is suggested to be calculated as a function of the height of the buildings without any computations of the peak displacements (Valles and Reinhorn 1997). Similarly to the Taiwan code, the Federal Emergency Management Agency suggests the determination of the minimum seismic gap as a percentage of the height of buildings in order to prevent their pounding during earthquakes (FEMA 1997).

Some of the regulations suggest to calculate the minimum seismic gap based simultaneously on peak structural displacements and height of structures. The Indian code for seismic design recalls the simple sum of peak displacements of adjacent buildings to be the base for calculating the minimum seismic separation gap together with a response reduction factor (IS 2002). The regulations from the Peru code for seismic design use values of the peak displacements of two adjacent buildings $\left(x_{\max}^L, x_{\max}^R\right)$ as well as the heights of structures as guides. In computing the minimum seismic gap, $d_{\min}$, the following formula is used (NBC 2003):

$$d_{\min} = \frac{2}{3}\left(x_{\max}^L + x_{\max}^R\right) \tag{6.2}$$

However, the calculated value from Eq. (6.2) can not be lower than (NBC 2003):

$$d_{\min} = 3 + 0.004(h - 500) \tag{6.3}$$

where h is the height of the lower building (in cm).

It is worth noting that all the above rules and formulae to calculate the minimum seismic gap in order to avoid earthquake-induced structural pounding can be related to four different forms of expressions (Valles and Reinhorn 1997):

$$d_{\min} \geq factor\left(sum(x_{\max}^L,\ x_{\max}^R)\right) \tag{6.4}$$

$$d_{\min} \geq factor(h^L,\ h^R) \tag{6.5}$$

$$d_{\min} \geq fixed\ distance \tag{6.6}$$

$$d_{\min} \geq SRSS(x_{\max}^L,\ x_{\max}^R) \tag{6.7}$$

6.2 Pounding Force Response Spectrum

In the case when earthquake-induced structural pounding can not be prevented, the design of neighbouring structures should include the appearance of additional forces due to collisions. The assessment of the peak pounding force value expected during the time of ground motion can be conducted with the use of pounding force response spectrum (see also Jankowski 2005, 2006). The spectrum may serve as a very useful tool for the design purposes of closely-spaced structures in seismic areas.

The displacement, velocity and acceleration response spectra are well known practical means of characterising earthquakes and their effects on structures. They allow an engineer to apply the knowledge of structural dynamics to the earthquake-resistant design in order to prevent or reduce structural damage. The response spectrum for a particular quantity is defined as a plot of the peak value of response quantity as a function of the natural vibration period of the system, or a related parameter such as frequency (Chopra 1995). The plot shows the peak response of the structure, modelled as an elastic single-degree-of-freedom (SDOF) system, for a specified value of structural damping. Among response spectra for different quantities, the displacement and acceleration response spectra are the most often used (ECS 1998). In order to predict the maximum relative displacement between two neighbouring structures with different natural periods, the relative displacement response spectrum was considered (Kawashima and Sato 1996). Ruangrassamee and Kawashima (2001) proposed also the concept of relative displacement response spectrum with pounding effect. In this section, the idea of pounding force spectrum for earthquake-induced structural pounding between two closely-spaced structures, modelled as SDOF systems (see Fig. 2.13), is considered.

6.2.1 Response Spectrum for One Existing and One New Structure

Let us first consider the situation when a new building is supposed to be constructed close to the existing one which has different dynamic characteristics. Assuming that the new structure is a right one and the existing building with known properties is a

left one, the pounding force response spectrum can be defined as a plot of the peak pounding force, $F_{\max}$, obtained for different values of T_2 under fixed values of ξ_{S2}, m_2 and d (Jankowski 2005):

$$F_{\max}(T_2, \xi_{S2}, m_2, d) = \max|F(t, T_2, \xi_{S2}, m_2, d)| \tag{6.8}$$

where T_2, ξ_{S2} and m_2 are the natural period, structural damping ratio and mass of the new (right) structure, respectively; d denotes the initial separation gap and t stands for time of the earthquake.

The elastic dynamic equation of motion for pounding-involved response of two structures modelled as SDOF systems (see Fig. 2.13) has been given in Eq. (2.22). The numerical study has been conducted in order to determine the pounding force response spectra for different values of damping ratio, ξ_2, and mass, m_2, of the new (right) structure as well as for various in-between gap sizes. When the effect of one parameter has been investigated, other parameters have remained unchanged. In the analysis, the following basic values describing the properties of the old (left) structure have been used: $m_1 = 10^6$ kg, $T_1 = 0.6$ s, $\xi_{S1} = 5\,\%$. The following values of the non-linear viscoelastic pounding force model's parameters have been applied in numerical simulations: $\bar{\beta} = 2.75 \times 10^9$ N/m$^{3/2}$, $\bar{\xi} = 0.35$ $(e = 0.65)$. The analysis has been conducted for different ground motion records. The examples of pounding force response spectra for the NS components of the El Centro earthquake are shown in Figs. 6.1 and 6.2. In particular, the pounding force response spectra for the gap size of 0.05 m for different values of mass and structural damping of the new structure are presented in Fig. 6.1, whereas Fig. 6.2 shows the pounding force response spectra for mass $m_2 = 10^6$ kg for different values of gap size and structural damping of the new structure.

The results of the study (see Figs. 6.1 and 6.2) show a significant influence of structural damping on peak pounding force obtained during the earthquake. This is obviously due to the fact that increasing damping leads to the reduction in structural vibrations and therefore reduction in the prior-impact velocities, which finally results in the lower values of pounding force. Moreover, it can be seen from Fig. 6.1 that the increase in the mass value of the new building results in substantial increase in the peak pounding force. On the other hand, the results presented in Fig. 6.2 indicate that the increase in the separation gap allows us to prevent collisions for a wider range of the natural vibration periods of the new structure. It is worth noting, however, that for the cases when impacts can not be prevented, the peak pounding forces are not substantially reduced as the gap size value increases.

6.2.2 Response Spectrum for Two New Structures

In this part of the chapter, let us consider the case of two new structures with different dynamic properties to be constructed one close to another (see some examples in Anagnostopoulos 1988; Chau et al. 2003; Karayannis and Favvata 2005;
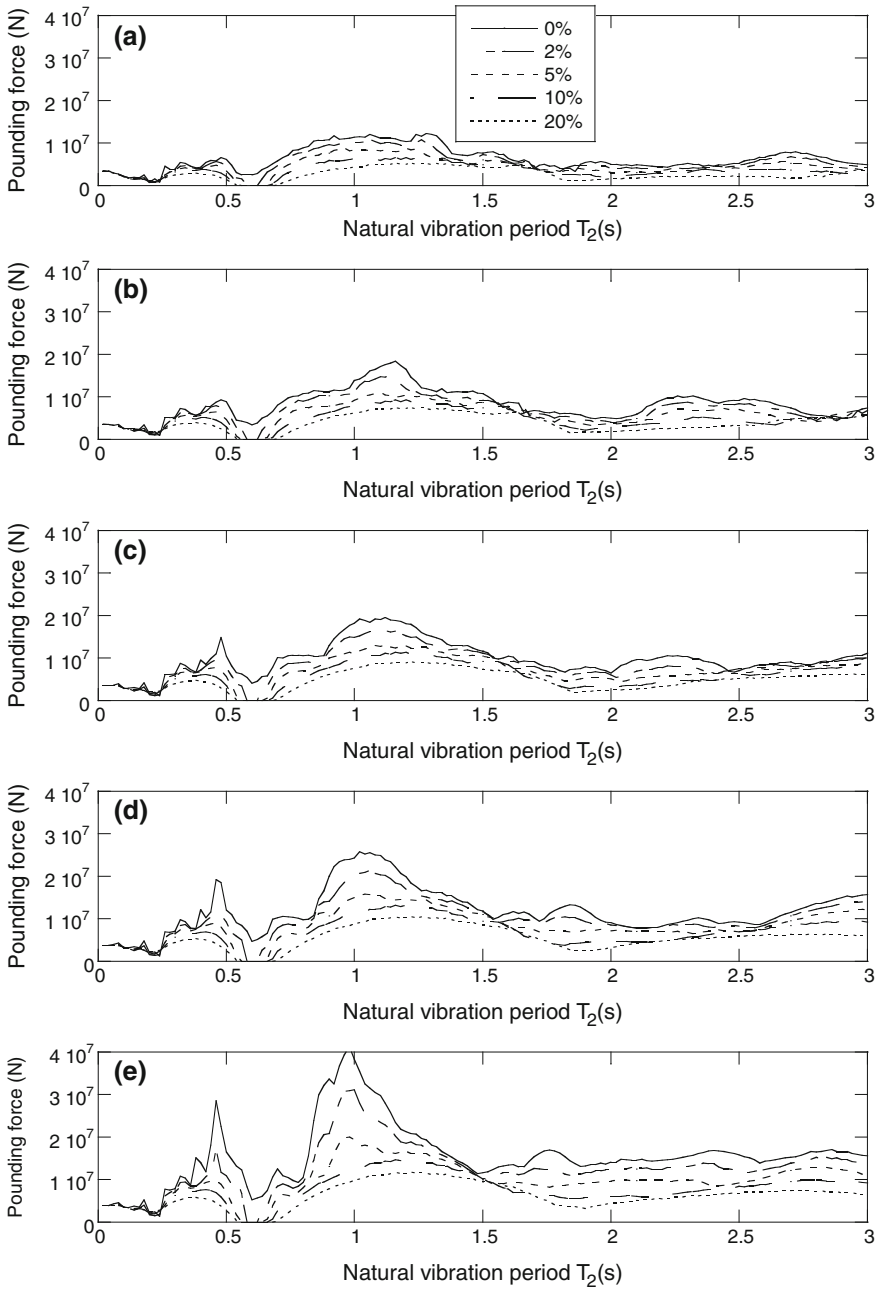
Fig. 6.1   Pounding force response spectra under the El Centro earthquake for different values of mass and structural damping ratio of the new structure (Jankowski 2005). **a** 200,000 kg. **b** 500,000 kg. **c** 1,000,000 kg. **d** 2,000,000 kg. **e** 5,000,000 kg
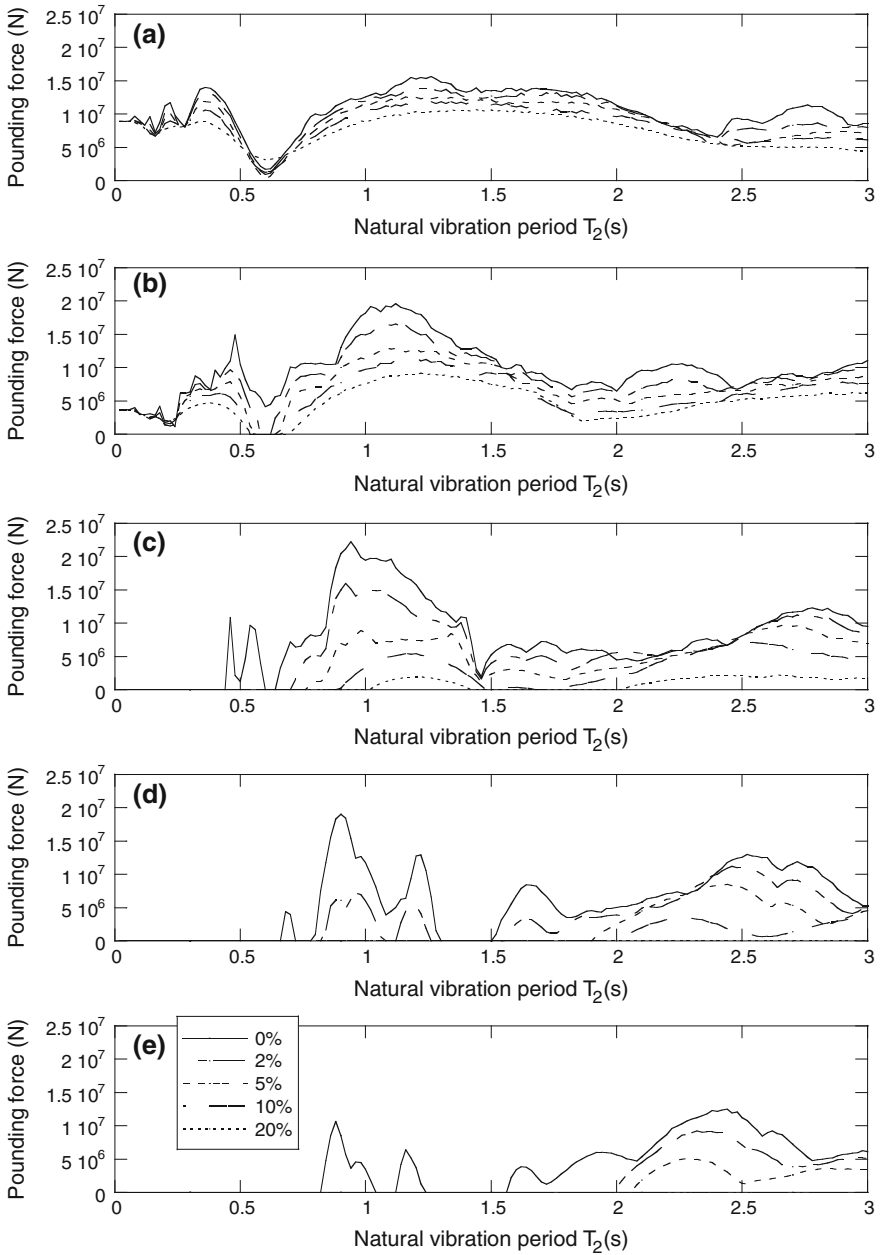
Fig. 6.2 Pounding force response spectra under the El Centro earthquake for different values of gap size and structural damping ratio of the new structure (Jankowski 2005). **a** 0 m. **b** 0.05 m. **c** 0.10 m. **d** 0.15 m. **e** 0.20 m

Jankowski 2007; Mahmoud and Jankowski 2009, 2011; Polycarpou and Komodromos 2010; Sołtysik and Jankowski 2013; Mahmoud et al. 2013). On the contrary to the response spectrum for one existing and one new building (Sect. 6.2.1), the pounding force response spectrum for two new structures will depend on properties of both of them. Moreover, in the case of long structures, such as buildings with spatially extended foundations, bridges or life-line systems, the incorporation of the spatial seismic effects, related to the propagation of seismic wave, might also be important (Der Kiureghian 1996; Zembaty 1997; Jankowski and Walukiewicz 1997; Jankowski and Wilde 2000; Dulińska 2011; Jankowski 2012). In this case, at least the influence of the wave passage effect, resulting in a time lag for the input earthquake records acting on two adjacent structures (or their parts), should be considered (see also Sect. 4.1). Then, the pounding force response spectrum can be defined as a plot of the peak pounding force, F_{max}, obtained for different values of T_1 and T_2 under fixed values of ξ_{S1}, ξ_{S2}, d, m_1, m_2, τ (Jankowski 2006):

$$F_{max}(T_1, T_2, \xi_{S1}, \xi_{S2}, d, m_1, m_2, \tau) = \max|F(t, T_1, T_2, \xi_{S1}, \xi_{S2}, d, m_1, m_2, \tau)| \quad (6.9)$$

where T_i, ξ_{Si} and m_i are the natural period, structural damping ratio and mass of structure i ($i = 1, 2$), respectively; d denotes the initial separation gap, τ is a time lag for the input ground motion records and t stands for time of the earthquake. It should be mentioned that, since the pounding force response spectrum defined in Eq. (6.9) is a plot against two natural vibration periods T_1, T_2 simultaneously, the spectrum has to be presented as a 3-dimensional graph (see also Ruangrassamee and Kawashima 2001), as obtained for a pair of two structural damping ratios ξ_{S1}, ξ_{S2}.

The elastic dynamic equation of motion for pounding-involved response of two structures modelled as SDOF systems (see Fig. 2.13) incorporating a time lag for the input ground motion records can be written as [compare Eq. (2.22)]:

$$\begin{bmatrix} m_1 & 0 \\ 0 & m_2 \end{bmatrix} \begin{bmatrix} \ddot{x}_1(t) \\ \ddot{x}_2(t) \end{bmatrix} + \begin{bmatrix} C_1 & 0 \\ 0 & C_2 \end{bmatrix} \begin{bmatrix} \dot{x}_1(t) \\ \dot{x}_2(t) \end{bmatrix} + \begin{bmatrix} K_1 & 0 \\ 0 & K_2 \end{bmatrix} \begin{bmatrix} x_1(t) \\ x_2(t) \end{bmatrix} + \begin{bmatrix} F(t) \\ -F(t) \end{bmatrix}$$
$$= -\begin{bmatrix} m_1 & 0 \\ 0 & m_2 \end{bmatrix} \begin{bmatrix} \ddot{x}_{g1}(t) \\ \ddot{x}_{g2}(t) \end{bmatrix} \quad (6.10)$$

where $x_i(t)$, $\dot{x}_i(t)$, $\ddot{x}_i(t)$ are the horizontal displacement, velocity and acceleration of structure i ($i = 1, 2$), respectively, C_i, K_i denote damping and stiffness coefficients, $\ddot{x}_{gi}(t)$ stands for the acceleration of input ground motion for ith structure and $F(t)$ is the pounding force.

The numerical study has been conducted in order to determine the pounding force response spectra for different values of damping ratios, masses, time lag of the input earthquake records as well as for various in-between gap sizes. When the effect of one parameter has been studied, other parameters have remained unchanged. In the analysis, the following basic values of structural model's parameters have been applied: $m_1 = m_2 = 10^6$ kg, $\xi_{S1} = \xi_{S2} = 5\%$, $d = 0.05$ m, $\tau = 0$ s. The following values of the non-linear viscoelastic pounding force model's

parameters have been applied in numerical simulations: $\bar{\beta} = 2.75 \times 10^9$ N/m$^{3/2}$, $\bar{\xi} = 0.35$ ($e = 0.65$). The analysis has been conducted for different ground motion records. The examples of pounding force response spectra for the NS component of the El Centro earthquake are shown in Figs. 6.3, 6.4, 6.5 and 6.6.

Figure 6.3 shows the pounding force response spectra for different values of identical structural damping ratios of both structures. As it can be seen from the figure, the influence of structural damping on the peak pounding force is substantial, similarly as in the case of spectra for one existing and one new structure (Sect. 6.2.1). For example, by comparing Fig. 6.3a with Fig. 6.3b, we can see that the increase in damping ratio for both structures from 0 to 2 % results in the decrease in the peak pounding force by 22 % in average (see also Jankowski 2006).
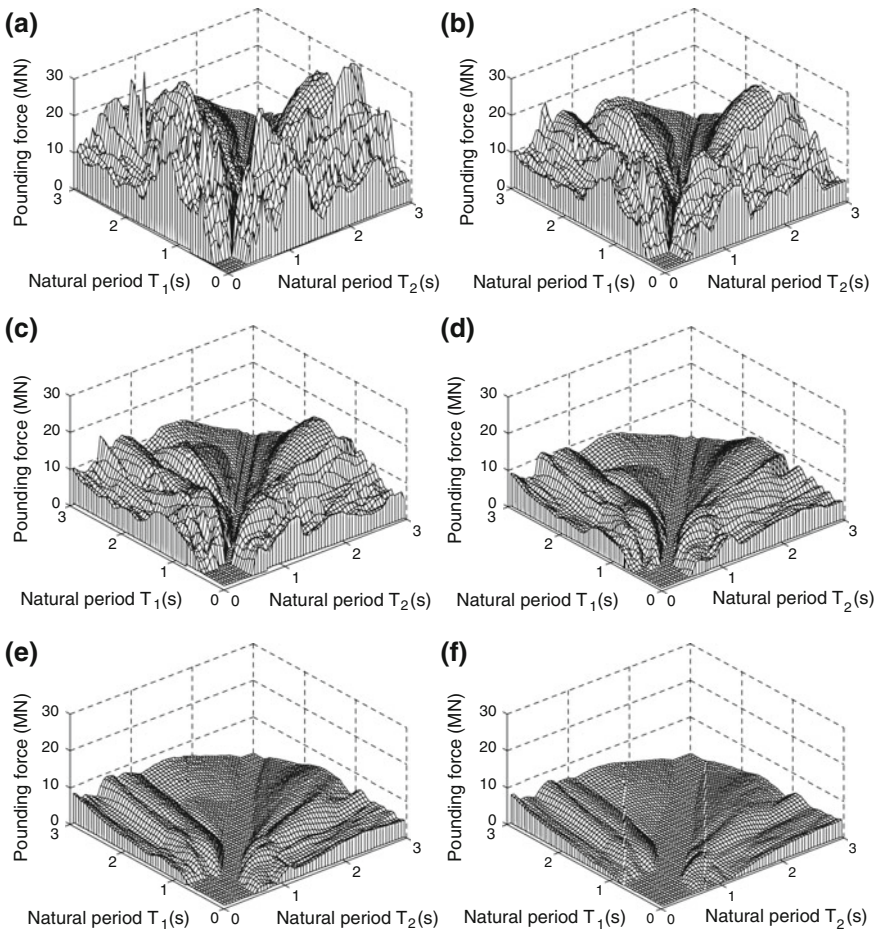

Fig. 6.3 Pounding force response spectra under the El Centro earthquake for different values of structural damping ratios of both structures (Jankowski 2006). **a** 0 %. **b** 2 %. **c** 5 %. **d** 10 %. **e** 15 %. **f** 20 %
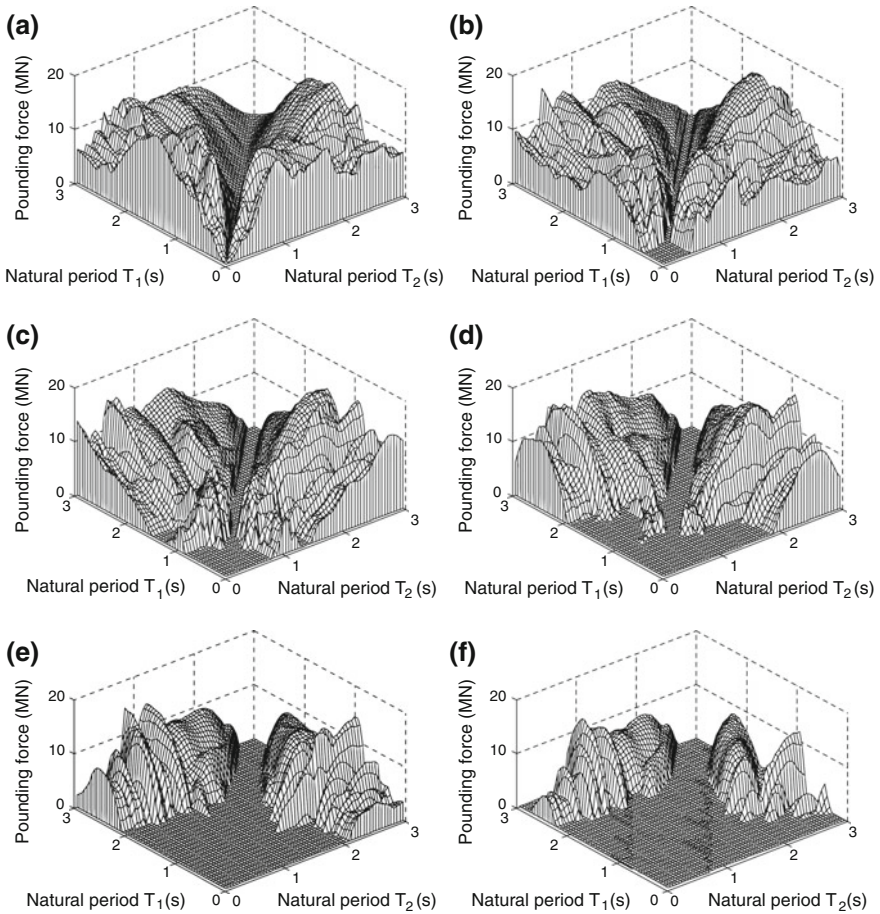
Fig. 6.4   Pounding force response spectra under the El Centro earthquake for different values of gap size between structures (Jankowski 2006). **a** 0 m. **b** 0.05 m. **c** 0.10 m. **d** 0.15 m. **e** 0.20 m. **f** 0.25 m

It can also be seen from Fig. 6.3 that the increase in structural damping results in extension of the region in the spectrum where the peak pounding force is equal to zero. This region is related to the cases when the natural vibration periods are very small for both structures (small displacements which do not lead to collisions) and when the natural periods are equal or nearly equal.

Pounding force response spectra for different values of gap size between structures are presented in Fig. 6.4. The spectra from the figure indicate that the increase in the separation gap allows us to prevent collisions for a wider range of the natural vibration periods of both structures. Actually, in the case of the El Centro earthquake, the gap size of 0.3 m is already sufficiently large to avoid impact for all structural periods analyzed. However, it should be underlined that for the
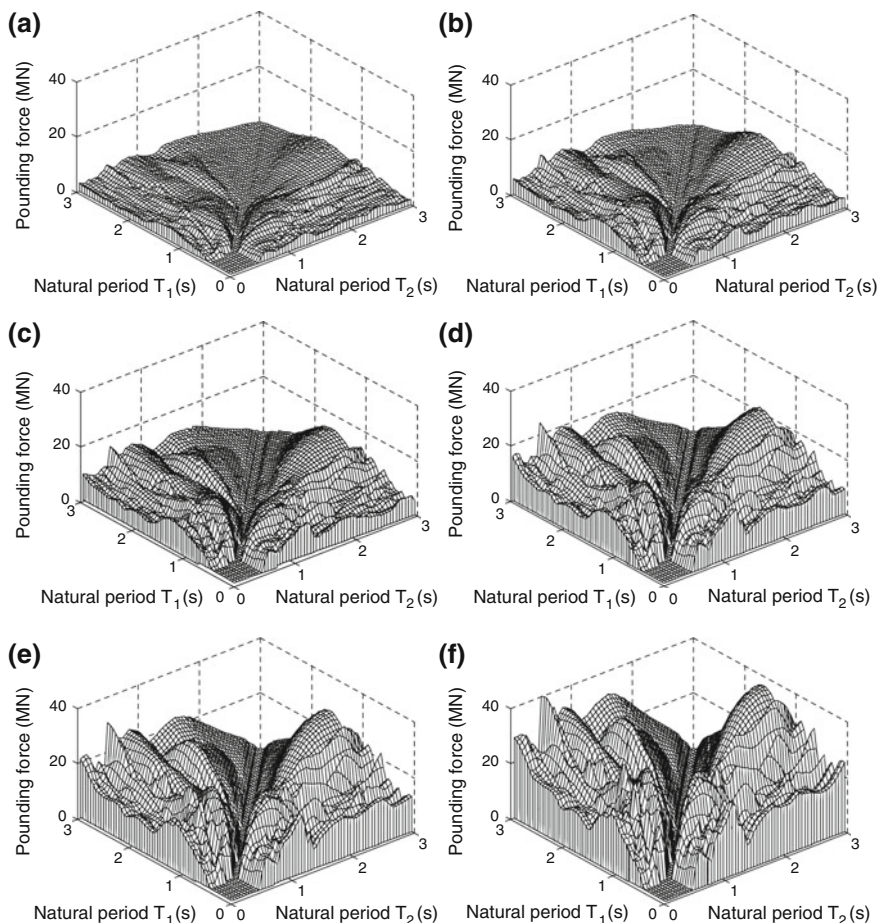
Fig. 6.5 Pounding force response spectra under the El Centro earthquake for different values of masses of both structures (Jankowski 2006). **a** 200,000 kg. **b** 500,000 kg. **c** 1,000,000 kg. **d** 2,000,000 kg. **e** 3,000,000 kg. **f** 5,000,000 kg

cases when pounding can not be prevented, the values of peak pounding force are nearly at the same level for different values of in-between gap size.

Figure 6.5 shows the pounding force response spectra for different values of identical masses of both structures. The figure confirms that the increase in the mass values leads to substantial increase in the peak pounding force. In the case of identical mass values of both structures, the shapes of the pounding force spectra are very similar with nearly linear, quite rapid increase in the peak pounding force values in the range of 200,000–5,000,000 kg (see also Jankowski 2006).

Pounding force response spectra for different values of time lag for the input earthquake records acting on two adjacent structures are shown in Fig. 6.6. The figure indicates that the time lag of at least 0.2 s leads to the disappearance of
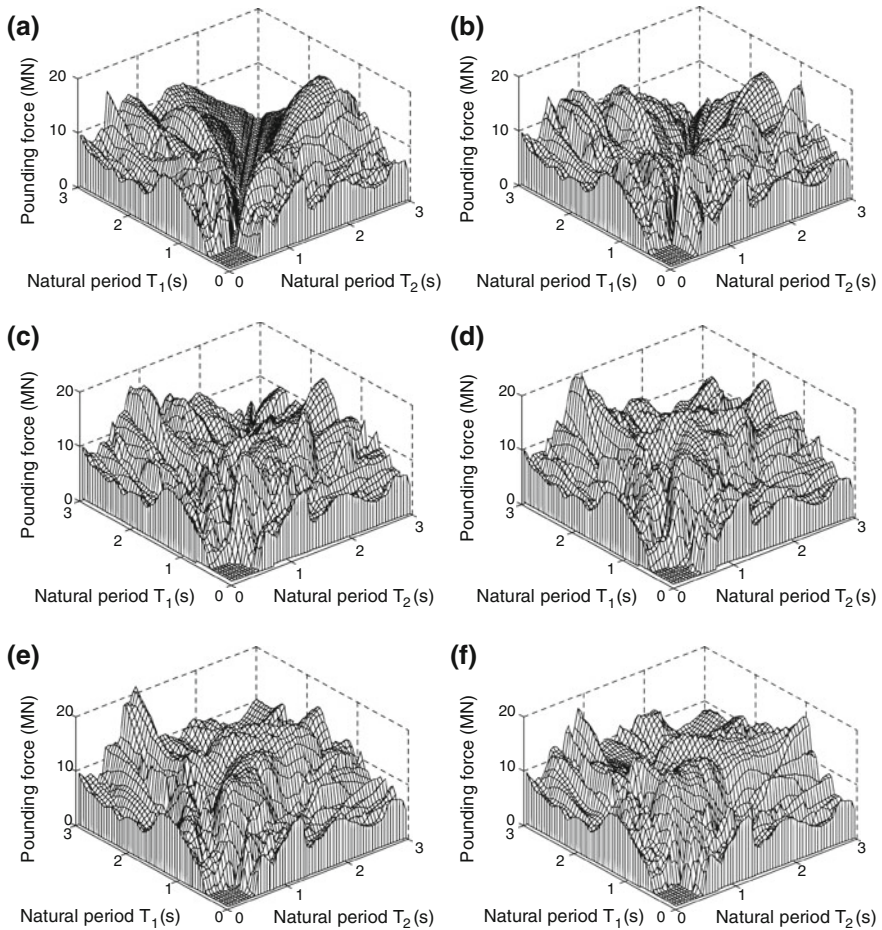
Fig. 6.6 Pounding force response spectra under the El Centro earthquake for different values of time lag for input ground motion records (Jankowski 2006). **a** 0 s. **b** 0.1 s. **c** 0.2 s. **d** 0.3 s. **e** 0.4 s. **f** 0.5 s

the region in the spectrum, in which the pounding force is equal to zero (observed for equal or nearly equal vibration periods of structures, see Figs. 6.3, 6.4 and 6.5). This behaviour results from the fact, that the seismic wave passage effect induces the out-of-phase vibrations even for structures with identical structural vibration periods. It can also be seen from Fig. 6.6 that the shapes of the pounding force response spectra do not change much for the time lag in the range of 0.2–0.5 s. Moreover, the region with zero pounding force observed in the case of very small natural vibration periods is nearly identical for all pounding force spectra apart from the value of time lag. This results from the fact, that the in-between gap size of 0.05 m is large enough to accommodate different, but very small vibrations of two analyzed structures.

6.3 Assessment of Structural Damage

In the design criteria, study against collapse is considered as the main objective. However, performance in terms of functionality and economy still plays important role. Great efforts are made to improve the methods of resistant design against dynamic loads due to earthquakes, not only to avoid failure during strong excitations but also to limit damage under moderate ground motions. The use of damage indices and damage measures for structures under dynamic loads are widely used and they can also be applied for the design purposes of colliding structures under seismic loads. They aim to clarify the different approach methodologies (Powell and Allahabadi 1988; Cosenza et al. 1993; Kappos 1997) and to detail different proposed formulations (McCabe and Hall 1989; Williams and Sexsmith 1995; Fardis 1995).

One of the key parameters used to identify structural damage is the kinematic and cyclic ductility, which can be defined as a function of rotation, curvature or displacement. The amount of kinematic energy dissipated during loading is another important aspect in structural damage.

One of the most often used damage index was proposed by Park and Ang (1985). It defines the structural damage in terms of the peak dynamic response (i.e. peak plastic displacement), as well as the hysteretic dissipated energy, and can be expressed as (see Park and Ang 1985; Park et al. 1985, 1987):

$$DI_{PA} = \frac{x_{\max}}{x_u} + \frac{\beta_{PA}}{F_Y x_u} \int dE \qquad (6.11)$$

where $x_{\max}$ is the peak displacement, x_u stands for the ultimate displacement, F_Y is the yield strength, dE denotes the incremental absorbed hysteretic energy and β_{PA} is a nonnegative constant. The level of damage can be defined based on the values of captured damage indices. A building can be considered to have insignificant damage for the assigned damage index $DI_{PA} \leq 0.2$, while for $DI_{PA} \leq 0.4$ damage can be considered as repairable. For $0.4 < DI_{PA} < 1$ damage can not be repairable, although the structure does not collapse and the case when $DI_{PA} \geq 1.0$ denotes total damage of the structure (Park and Ang 1985; Park et al. 1987).

Powell and Allahabadi (1988) proposed a damage index in terms of the peak plastic displacement, independent from the amount of dissipated energy. The formula used to define the damage index, DI_{AP}, can be written as (Powell and Allahabadi 1988):

$$DI_{AP} = \frac{x_{\max} - x_y}{x_u - x_y} \qquad (6.12)$$

where x_y is the yield displacement.

Damage indices based on the kinematic or cyclic ductility, as a measure for damage, assume that structural model collapse is mainly due to the induced peak plastic displacement neglecting the effect of a number of plastic cycles and the

energy dissipated under the applied dynamic load. However, it has been shown that these indices can be used for structures with cumulative deterioration, such as in the case of impulse-type or short-duration earthquakes which are characterized by one cycle with a large plastic displacement and other cycles with a small amount of plastic work.

A damage index based on the structure hysteretic energy was proposed by Fajfar (1992) and Cosenza et al. (1993) and can be expressed as:

$$DI_{FC} = \frac{E_H}{F_Y x_y (\mu_u - 1)} \tag{6.13}$$

where E_H and μ_u are the dissipated hysteretic energy and ultimate ductility factor, respectively.

Another measure of structural performance is given as the dissipated hysteretic energy normalized to the input energy of the structure. This index is defined as (Bojórquez et al. 2010; Moustafa 2011):

$$DI_H = \frac{E_H}{E_I} \tag{6.14}$$

where E_I denotes the earthquake input energy, considering the fact that the ground starts shaking until it comes to rest. Note that the damage index of Eq. (6.14) includes the structure's response demanded by the ground motion and the associated structural capacity parameters in an implicit form. Note also that DI_H close to zero implies a linear behaviour, while DI_H larger than zero indicates inelastic behaviour and occurrence of structural damage.

All the aforementioned damage indices are considered in the two successive sections concerning the numerical simulations of earthquake-induced response and damage assessment of two colliding buildings with fixed bases (non-isolated structures) and with isolated bases (base-isolated structures).

6.3.1 Damage Indices in Non-isolated Buildings

For the purposes of the analysis focused on non-isolated buildings, let us use the simplified SDOF structural model shown in Fig. 2.13. The dynamic equation of motion for such a model, considering inelastic (elastic-perfectly plastic) behaviour of both buildings, can be written as [compare Eqs. (2.22) and (3.1)]:

$$\mathbf{M}\ddot{\mathbf{x}}(t) + \mathbf{C}\dot{\mathbf{x}}(t) + \mathbf{F}_S(t) + \mathbf{F}(t) = -\mathbf{M}\mathbf{1}\ddot{x}_g(t) \tag{6.15a}$$

$$\mathbf{M} = \begin{bmatrix} m_1 & 0 \\ 0 & m_2 \end{bmatrix}; \quad \mathbf{C} = \begin{bmatrix} C_1 & 0 \\ 0 & C_2 \end{bmatrix}; \quad \ddot{\mathbf{x}}(t) = \begin{bmatrix} \ddot{x}_1(t) \\ \ddot{x}_2(t) \end{bmatrix}; \quad \dot{\mathbf{x}}(t) = \begin{bmatrix} \dot{x}_1(t) \\ \dot{x}_2(t) \end{bmatrix}$$

(6.15b)

$$\mathbf{F}_S(t) = \begin{bmatrix} F_{S1}(t) \\ F_{S2}(t) \end{bmatrix}; \quad \mathbf{F}(t) = \begin{bmatrix} F(t) \\ -F(t) \end{bmatrix}; \quad \mathbf{1} = \begin{bmatrix} 1 \\ 1 \end{bmatrix} \qquad (6.15c)$$

where $x_i(t)$, $\dot{x}_i(t)$, $\ddot{x}_i(t)$ are the horizontal displacement, velocity and acceleration of building i ($i = 1, 2$), respectively, $F_{Si}(t)$ is the inelastic shear force equal to $F_{Si}(t) = K_i x_i(t)$ for the elastic range till the yield strength F_{Yi} is reached and $F_{Si}(t) = \pm F_{Yi}$ for the plastic range, K_i, C_i denote elastic structural stiffness and damping coefficients, $\ddot{x}_g(t)$ stands for the acceleration of input ground motion and $F(t)$ is the pounding force, which is equal to zero when $\delta(t) \leq 0$ and is defined by Eq. (2.16) if $\delta(t) > 0$, where deformation $\delta(t)$ is defined by Eq. (2.23).

As the example, two buildings with the basic dynamic parameters described in Sect. 3.1 have been used in the analysis. Furthermore, the yield strength for the left and the right inelastic buildings have been taken as $F_{Y1} = 1.369 \times 10^5$ N and $F_{Y2} = 1.442 \times 10^7$ N, respectively. The initial separation gap between buildings has been set to $d = 0.05$ m and has been changed later to study its effect on damage of adjacent buildings. The following values of the non-linear viscoelastic pounding force model's parameters have been applied in the analysis: $\bar{\beta} = 2.75 \times 10^9$ N/m$^{3/2}$, $\bar{\xi} = 0.35$ ($e = 0.65$). The time-stepping Newmark method (Newmark 1959) with constant time step $\Delta t = 0.002$ s has been used in order to solve the equation of motion (6.15a–c) numerically. A set of 9 earthquake ground motion records listed in Table 5.1 have been used as input excitations. In the numerical analysis, all acceleration records have been scaled to have the peak ground acceleration of 0.5 g (g stands for the acceleration of gravity) to ensure inelastic response of structures. The parameters of the damage indices have been taken as: $\mu_{u1} = \mu_{u2} = 0.6$ and $\beta_{PA} = 0.15$.

The examples of numerical results, in the form of different damage indices time histories for colliding non-isolated buildings under the El Centro earthquake, are shown in Figs. 6.7, 6.8, 6.9 and 6.10. Additionally, the values of peak damage indices for the left and the right structure under all analyzed ground motion records are summarized in Tables 6.1 and 6.2, respectively (see also Moustafa and Mahmoud 2014). The results of the study indicate that the El Centro, Loma Prieta, Duzce and Kobe earthquakes are among the ground motions which produce the largest damage indices. This could be attributed to the characteristics of these records since they have rich frequency contents, high energy and small source-site distance (near-fault records). In fact, according to the values of Park and Ang damage index for the Loma Prieta and Kobe earthquakes, both buildings are totally collapsed. On the other hand, other earthquake records, especially the Nahanni and San Fernando ground motions, produce much lower damage indices (either repairable damage or damage beyond repair but total collapse does not occur).
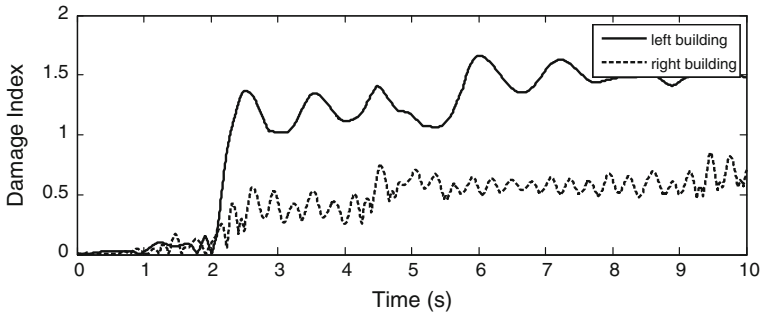
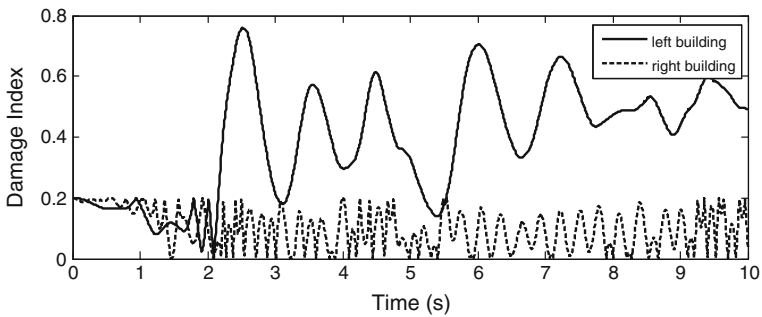**Fig. 6.7** Park and Ang damage index time histories for non-isolated buildings under the El Centro earthquake

Fig. 6.8 Powell and Allahabadi damage index time histories for non-isolated buildings under the El Centro earthquake
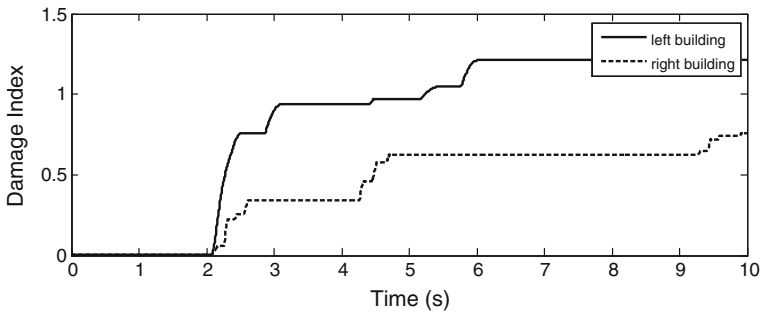

Fig. 6.9 Fajfar and Cosenza damage index time histories for non-isolated buildings under the El Centro earthquake

It can also be seen from Figs. 6.7, 6.8, 6.9 and 6.10 that, in the case of the El Centro earthquake, the values of damage indices for the left building (lighter and more flexible) are substantially larger than for the right structure (heavier and stiffer).
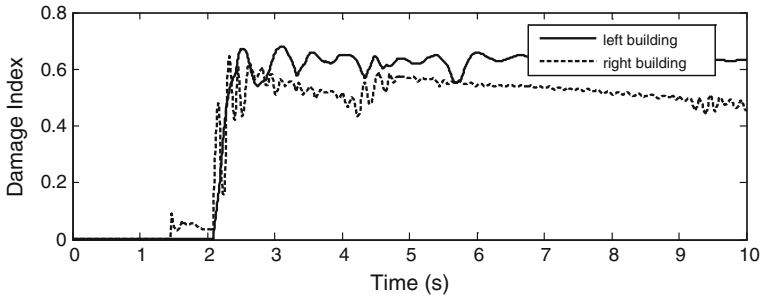
Fig. 6.10 Time histories of damage index based on hysteric energy for non-isolated buildings under the El Centro earthquake

Table 6.1 Peak damage indices for the left non-isolated building under different ground motions

Earthquake	DI_{PA}	DI_{AP}	DI_{FC}	DI_H
El Centro	1.6616	0.7582	1.2100	0.6804
Kocaeli	0.5421	0.2033	0.2743	0.4122
LomaPrieta	1.2138	0.6614	0.6614	0.5441
Duzce	1.4382	0.7898	0.8211	0.7128
Kobe	1.9882	0.8579	1.5627	0.7472
Tabas	0.6043	0.2508	0.3069	0.3354
Nahanni	0.1141	0.2000	0.1226	0.1708
SanFernando	0.4422	0.2000	0.2182	0.7473
Northridge	0.2570	0.2000	0.0571	0.4150

Table 6.2 Peak damage indices for the right non-isolated building under different ground motions

Earthquake	DI_{PA}	DI_{AP}	DI_{FC}	DI_H
El Centro	0.8498	0.2000	0.7568	0.6455
Kocaeli	0.9671	0.2734	0.8863	0.6311
LomaPrieta	1.2390	0.3084	1.1846	0.8545
Duzce	0.8972	0.2000	0.8426	0.5393
Kobe	1.4275	0.2360	1.4685	0.7597
Tabas	0.3170	0.2459	0.1370	0.5240
Nahanni	0.3809	0.2000	0.1508	0.3538
SanFernando	0.4466	0.2000	0.3083	0.3445
Northridge	1.0226	0.2805	1.0889	0.5288

However, this relation is not the same for other ground motions (compare Table 6.1 with Table 6.2) and might be even reversed, as it is in the case of the Kocaeli earthquake for example.

In order to examine the effect of the separation distance on damage indices of colliding non-isolated buildings, the parametric study has been conducted. The value of the gap size between adjacent structures has been varied between 0 and 0.20 m and the responses of both buildings have been determined for each
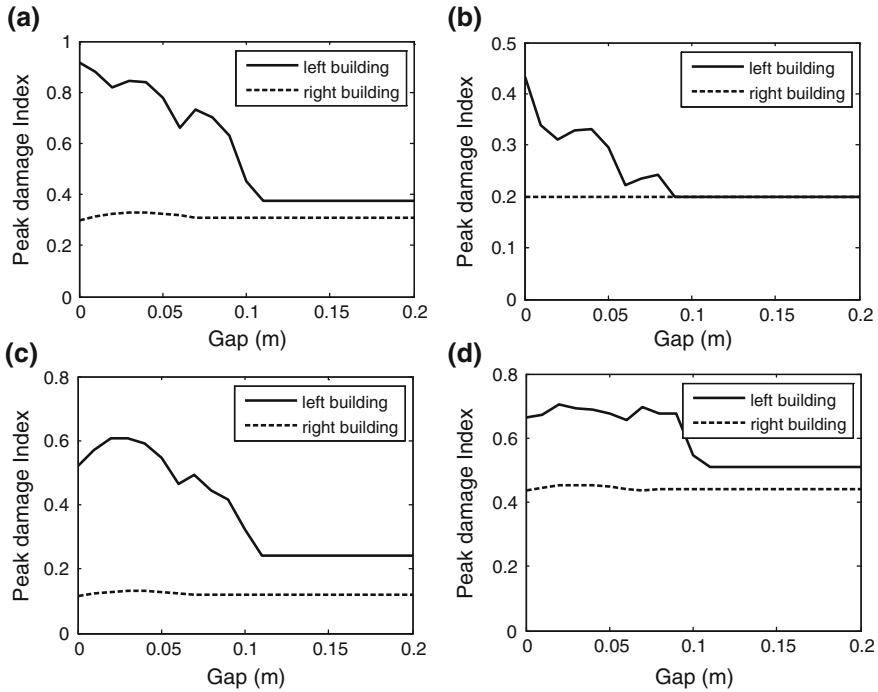
Fig. 6.11 Peak damage indices for non-isolated buildings under the El Centro earthquake with respect to the gap size. **a** Park & Ang. **b** Powell & Allahabadi. **c** Fajfar & Cosenza. **d** Hysteretic

separation distance. Figure 6.11 shows the peak damage indices for both non-isolated buildings under the scaled El Centro earthquake. It should be underlined that, in the case of the ground motion considered, pounding does not occur for a gap size of 0.11 m, which is large enough to prevent collisions. It can be seen from Fig. 6.11 that, starting from this value of the separation distance, damage indices for adjacent buildings are stabilized with constant values. On the other hand, in the range when pounding take place, i.e. between 0 and 0.11 m, structural interactions contribute to the significant increase in damage indices for the left building. It can be seen from the figure that the influence of the gap size on damage indices for this structure is substantial with the general trend of reduction in values of damage indices when the gap size increases.

6.3.2 Damage Indices in Base-Isolated Buildings

For the purposes of the analysis focused on the base-isolated buildings, let us use the simplified structural model shown in Fig. 6.12. The dynamic equation of motion for such a model, considering inelastic (elastic-perfectly plastic) behaviour of both buildings, can be written as [compare Eqs. (6.15a–6.15c) and Eq. (3.6)]:
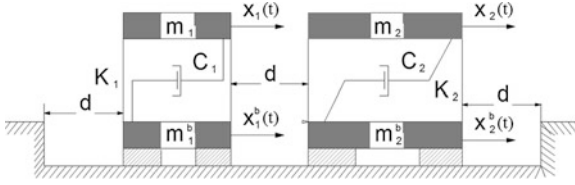
Fig. 6.12 Model of colliding base-isolated buildings

$$\mathbf{M}\ddot{\mathbf{x}}(t) + \mathbf{C}(t)\dot{\mathbf{x}}(t) + \mathbf{F}_S(t) + \mathbf{F}(t) = -\mathbf{M1}\ddot{x}_g(t) \tag{6.16a}$$

$$\mathbf{M} = \begin{bmatrix} m_1^b & 0 & 0 & 0 \\ 0 & m_1 & 0 & 0 \\ 0 & 0 & m_2^b & 0 \\ 0 & 0 & 0 & m_2 \end{bmatrix}; \quad \ddot{\mathbf{x}}(t) = \begin{bmatrix} \ddot{x}_1^b(t) \\ \ddot{x}_1(t) \\ \ddot{x}_2^b(t) \\ \ddot{x}_2(t) \end{bmatrix}; \quad \dot{\mathbf{x}}(t) = \begin{bmatrix} \dot{x}_1^b(t) \\ \dot{x}_1(t) \\ \dot{x}_2^b(t) \\ \dot{x}_2(t) \end{bmatrix} \tag{6.16b}$$

$$\mathbf{C}(t) = \begin{bmatrix} C_1^b(t) + C_1 & -C_1 & 0 & 0 \\ -C_1 & C_1 & 0 & 0 \\ 0 & 0 & C_2^b(t) + C_2 & -C_2 \\ 0 & 0 & -C_2 & C_2 \end{bmatrix}; \tag{6.16c}$$

$$\mathbf{F}_S(t) = \begin{bmatrix} K_1^b(t)x_1^b(t) - F_{S1}(t) \\ F_{S1}(t) \\ K_2^b(t)x_2^b(t) - F_{S2}(t) \\ F_{S2}(t) \end{bmatrix}; \quad \mathbf{F}(t) = \begin{bmatrix} F_b(t) \\ F(t) \\ -F_b(t) \\ -F(t) \end{bmatrix}; \quad \mathbf{1} = \begin{bmatrix} 1 \\ 1 \\ 1 \\ 1 \end{bmatrix} \tag{6.16d}$$

where, m_i^b, $\ddot{x}_i^b(t)$, $\dot{x}_i^b(t)$ are the mass, acceleration and velocity of the base of building i ($i = 1, 2$), respectively; $K_i^b(t)$, $C_i^b(t)$ are stiffness and damping coefficients for isolation devices and $F_b(t)$ is the pounding force at the base level [see Eq. (2.16)].

As the example, two buildings with the basic dynamic parameters described in Sect. 3.1 have been used in the analysis. Furthermore, the yield strength for the left and the right inelastic buildings have been taken as $F_{Y1} = 1.369 \times 10^5$ N and $F_{Y2} = 1.442 \times 10^7$ N, respectively. It has been assumed that the isolation system consists of High Damping Rubber Bearings (HDRBs). In order to simulate the behaviour of the devices, a non-linear strain-rate dependent model has been applied in the analysis [see Eq. (3.4)]. The left building has been equipped with 4 circular HDRBs, with the parameters of the bearing's model described in Sect. 3.3.1 (see also example 3 in Jankowski 2003) and the right building with 4 square HDRBs, with the parameters of the bearing's model described in Sect. 3.3.2 (see also example 1 in Jankowski 2003). The initial separation gap between buildings has been set to $d = 0.05$ m and has been changed later to study its effect on damage of

adjacent buildings. The following values of the non-linear viscoelastic pounding force model's parameters have been applied in the analysis: $\bar{\beta} = 2.75 \times 10^9$ N/m$^{3/2}$, $\bar{\bar{\xi}} = 0.35$ ($e = 0.65$). The time-stepping Newmark method with constant time step $\Delta t = 0.002$ s has been used in order to solve the equation of motion (6.16a–6.16d) numerically. A set of 9 earthquake ground motion records listed in Table 5.1 have been used as input excitations. Similarly as in Sect. 6.3.1, all acceleration records have been scaled to have the peak ground acceleration of 0.5 g to ensure inelastic response of structures. The parameters of the damage indices have been taken as: $\mu_{u1} = \mu_{u2} = 0.6$ and $\beta_{PA} = 0.15$.

The examples of numerical results, in the form of different damage indices time histories for colliding base-isolated buildings under the El Centro earthquake, are shown in Figs. 6.13, 6.14, 6.15 and 6.16. Additionally, the values of peak damage indices for the left and the right structure under all analyzed ground motion records are summarized in Tables 6.3 and 6.4, respectively (see also Moustafa and Mahmoud 2014). The results of the study reveal that damage indices are considerably
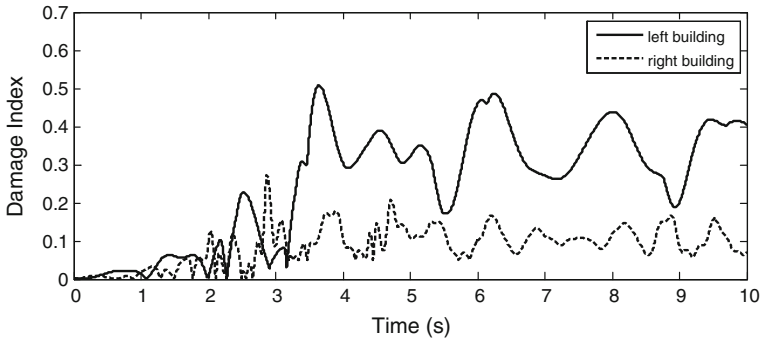

Fig. 6.13 Park and Ang damage index time histories for base-isolated buildings under the El Centro earthquake
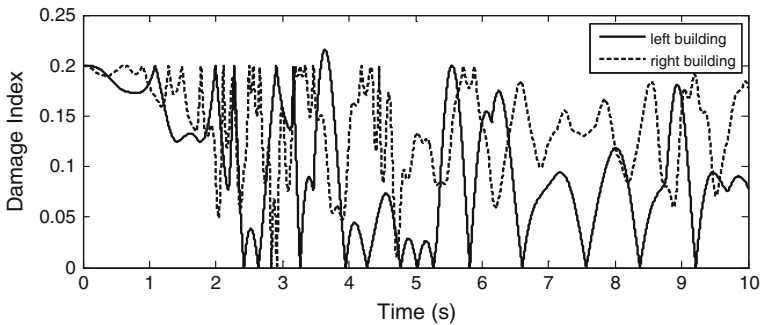

Fig. 6.14 Powell and Allahabadi damage index time histories for base-isolated buildings under the El Centro earthquake
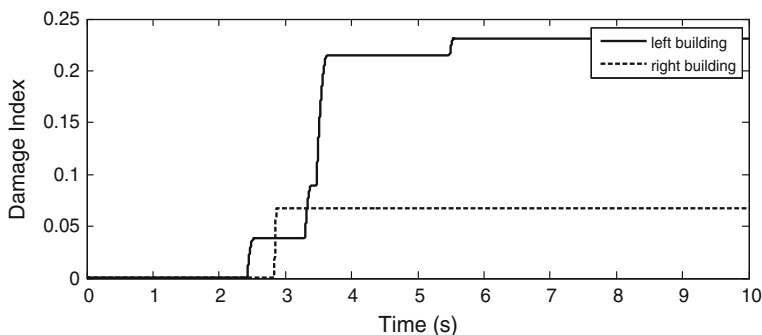
Fig. 6.15 Fajfar and Cosenza damage index time histories for base-isolated buildings under the El Centro earthquake
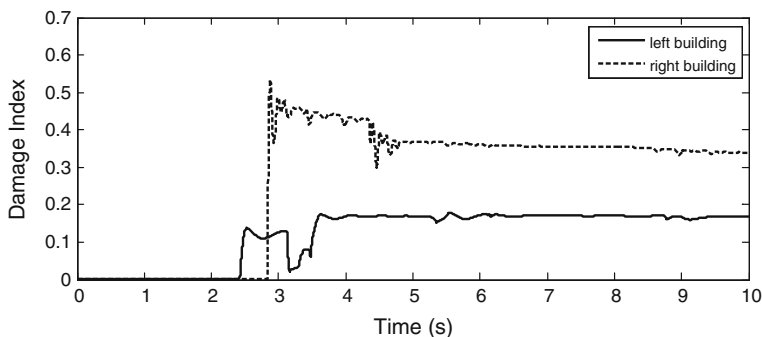

Fig. 6.16 Time histories of damage index based on hysteric energy for base-isolated buildings under the El Centro earthquake

Table 6.3 Peak damage indices for the left base-isolated building under different ground motions

Earthquake	DI_{PA}	DI_{AP}	DI_{FC}	DI_H
El Centro	1.9011	0.9670	1.2624	0.5104
Kocaeli	1.0323	0.5467	0.5467	0.6335
LomaPrieta	0.4050	0.2000	0.2306	0.5665
Duzce	1.3632	0.7557	0.7557	0.5205
Kobe	1.3929	0.6570	1.4542	0.6461
Tabas	0.5274	0.2000	0.2941	0.4410
Nahanni	0.0858	0.2000	0.0000	0.0000
SanFernando	0.9885	0.4396	0.6244	0.7903
Northridge	0.3470	0.2000	0.1139	0.4353

different for base-isolated structures as compared to the values obtained for the non-isolated buildings. This is due to the fact that adding isolation devices results in considerable changes of structural natural frequencies. Tables 6.3 and 6.4 indicate

Table 6.4 Peak damage indices for the right base-isolated building under different ground motions

Earthquake	DI_{PA}	DI_{AP}	DI_{FC}	DI_H
El Centro	1.1359	0.3419	1.2559	0.8208
Kocaeli	0.3756	0.2000	0.1690	0.7059
LomaPrieta	0.6049	0.2768	0.3661	0.8333
Duzce	1.2335	0.6738	1.1652	0.8231
Kobe	3.4340	1.4861	3.2333	0.8351
Tabas	0.2942	0.2000	0.0806	0.2761
Nahanni	0.0718	0.2000	0.0000	0.0000
SanFernando	0.6777	0.3227	0.3228	0.8575
Northridge	0.1949	0.2000	0.0178	0.3194

that the El Centro, Kocaeli, Duzce and Kobe earthquakes are among the ground motions which produce the largest damage indices in the case of base-isolated buildings. On the other hand, other earthquake records, especially the Nahanni and Northridge ground motions, produce much lower damage indices. Moreover, similarly as in the case of non-isolated structures, damage indices for the left base-isolated building might be either higher or lower than the values determined for the right structure with the base isolation.
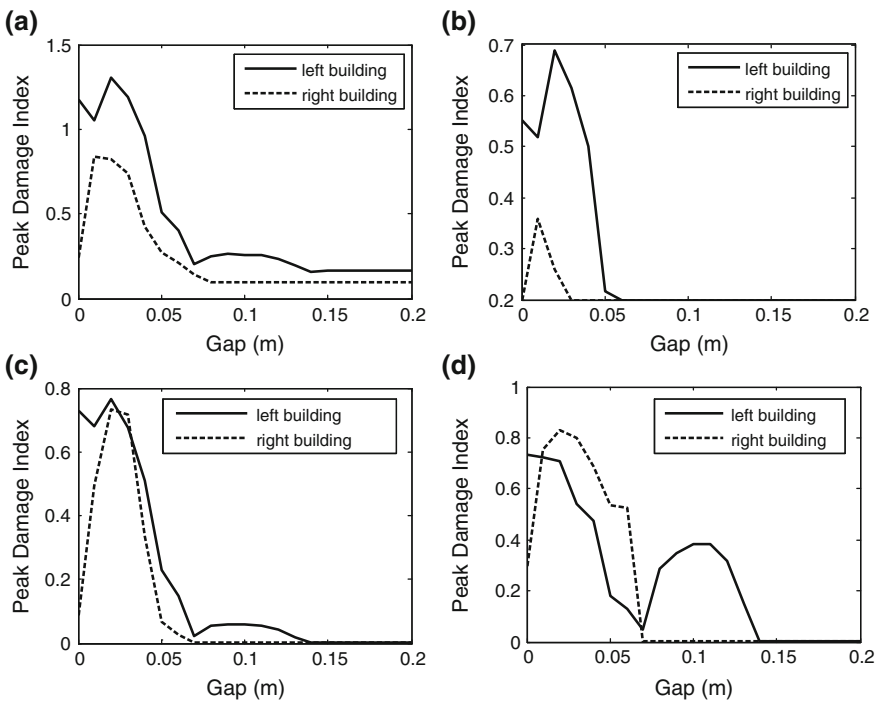

Fig. 6.17 Peak damage indices for base-isolated buildings under the El Centro earthquake with respect to the gap size. **a** Park and Ang. **b** Powell and Allahabadi. **c** Fajfar and Cosenza. **d** Hysteretic

In order to examine the effect of the separation distance on damage indices of colliding base-isolated buildings, the parametric study has also been conducted. Similarly as in Sect. 6.3.1, the value of the gap size between adjacent structures has been varied between 0 and 0.20 m. Figure 6.17 shows the peak damage indices for both base-isolated buildings under the scaled El Centro earthquake. It should be underlined that, this time, pounding does not occur for a gap size of 0.14 m, which is larger than for non-isolated buildings because of the fact that base-isolated structures experience larger response displacements (Kelly 1993; Komodromos 2000; Nagarajaiah and Sun 2001; Agarwal et al. 2007; Komodromos et al. 2007; Mahmoud et al. 2012; Falborski and Jankowski 2013). It can be seen from Fig. 6.17 that, starting from this value of the separation distance, damage indices for adjacent buildings are stabilized with constant values. On the other hand, in the range when pounding take place, i.e. between 0 and 0.14 m, the curves of damage indices for both structures show initially the increase trend and then their values decrease with the increase in the separation gap. Anyway, the results clearly indicate that structural interactions contribute to the significant increase in damage indices of both base-isolated buildings.

References

Agarwal, V.K., Niedzwecki, J.M., van de Lindt, J.W.: Earthquake induced pounding in friction varying base isolated buildings. Eng. Struct. 29, 2825–2832 (2007)

Anagnostopoulos, S.A.: Pounding of buildings in series during earthquakes. Earthquake Eng. Struct. Dynam. 16, 443–456 (1988)

ASCE: Minimum Design Loads for Buildings and other Structures SEI/ASCE 7-02. American Society of Civil Engineers, USA (2010)

Bojórquez, E., Reyes-Salazar, A., Terán-Gilmore, A., Ruiz, S.E.: Energy-based damage index for steel structures. Steel Compos. Struct. 10, 343–360 (2010)

Chau, K.T., Wei, X.X., Guo, X., Shen, C.Y.: Experimental and theoretical simulations of seismic poundings between two adjacent structures. Earthquake Eng. Struct. Dynam. 32, 537–554 (2003)

Chopra, A.K.: Dynamics of Structures: Theory and Applications to Earthquake Engineering. Prentice-Hall, Englewood Cliffs, USA (1995)

Cosenza, E., Manfredi, G., Ramasco, R.: The use of damage functionals in earthquake engineering: a comparison between different procedures. Earthquake Eng. Struct. Dynam. 22, 855–868 (1993)

Der Kiureghian, A.: A coherency model for spatially varying ground motions. Earthquake Eng. Struct. Dynam. 25, 99–111 (1996)

Dulińska, J.M.: Influence of wave velocity in the ground on dynamic response of large dimensional structures. Int. J. Earth Sci. Eng. 4, 538–541 (2011)

ECS: Eurocode 8: Design Provisions for Earthquake Resistance of Structures. European Committee for Standardization, Brussels, Belgium (1998)

Fajfar, P.: Equivalent ductility factors, taking into account low-cycle fatigue. Earthquake Eng. Struct. Dynam. 21, 837–848 (1992)

Falborski, T., Jankowski, R.: Polymeric bearings—a new base isolation system to reduce structural damage during earthquakes. Key Eng. Mater. 569–570, 143–150 (2013)

Fardis M.: Damage measures and failure criteria for reinforced concrete members. In: Proceedings of 10th European Conference on Earthquake Engineering. Vienna, Austria, 28 August–2 September 1994, Rotterdam, Netherlands: Balkema, pp. 1377–1382 (1995)

FEMA: NEHRP Guidelines for the Seismic Rehabilitation of Buildings. Federal Emergency Management Agency, FEMA Publication 273, USA (1997)

IBC: International Building Code. International Code Council Inc., USA (2003)

IBC: International Building Code. International Code Council Inc., USA (2009)

IS: Indian Standard. Criteria for Earthquake Resistant Design of Structures. IS 1893–2002. Bureau of Indian standards, India (2002)

Jankowski, R.: Nonlinear rate dependent model of high damping rubber bearing. Bull. Earthq. Eng. **1**, 397–403 (2003)

Jankowski, R.: Impact force spectrum for damage assessment of earthquake-induced structural pounding. Key Eng. Mater. **293–294**, 711–718 (2005)

Jankowski, R.: Pounding force response spectrum under earthquake excitation. Eng. Struct. **28**, 1149–1161 (2006)

Jankowski, R.: Assessment of damage due to earthquake-induced pounding between the main building and the stairway tower. Key Eng. Mater. **347**, 339–344 (2007)

Jankowski, R.: Non-linear FEM analysis of pounding-involved response of buildings under non-uniform earthquake excitation. Eng. Struct. **37**, 99–105 (2012)

Jankowski, R., Walukiewicz, H.: Modeling of two-dimensional random fields. Probab. Eng. Mech. **12**, 115–121 (1997)

Jankowski, R., Wilde, K.: A simple method of conditional random field simulation of ground motions for long structures. Eng. Struct. **22**, 552–561 (2000)

Kappos, A.J.: Seismic damage indices for RC buildings: evaluation of concepts and procedures. Prog. Struct. Mat. Eng. **1**, 78–87 (1997)

Karayannis, C.G., Favvata, M.J.: Earthquake-induced interaction between adjacent reinforced concrete structures with non-equal heights. Earthquake Eng. Struct. Dynam. **34**, 1–20 (2005)

Kawashima, K., Sato, T.: Relative displacement response spectrum and its application. In: Eleventh World Conference on Earthquake Engineering, paper no. 1103. Acapulco, Mexico, 23–28 June 1996

Kelly, J.M.: Earthquake-Resistant Design with Rubber. Springer, London, UK (1993)

Komodromos, P.: Seismic isolation of earthquake-resistant structures. WIT Press, Southanpton, UK (2000)

Komodromos, P., Polycarpou, P.C., Papaloizou, L., Phocas, M.C.: Response of seismically isolated buildings considering poundings. Earthquake Eng. Struct. Dynam. **36**, 1605–1622 (2007)

Mahmoud, S., Abd-Elhamed, A., Jankowski, R.: Earthquake-induced pounding between equal height multi-storey buildings considering soil-structure interaction. Bull. Earthq. Eng. **11**(4), 1021–1048 (2013)

Mahmoud, S., Austrell, P.-E., Jankowski, R.: Simulation of the response of base-isolated buildings under earthquake excitations considering soil flexibility. Earthquake Eng. Eng. Vibr **11**, 359–374 (2012)

Mahmoud, S., Jankowski, R.: Elastic and inelastic multi-storey buildings under earthquake excitation with the effect of pounding. J. Appl. Sci. **9**(18), 3250–3262 (2009)

Mahmoud, S., Jankowski, R.: Modified linear viscoelastic model of earthquake-induced structural pounding. Iran J. Sci. Technol. **35**(C1), 51–62 (2011)

McCabe, S., Hall, W.: Assessment of seismic structural damage. J. Struct. Eng. **115**, 2166–2183 (1989)

Moustafa, A.: Damage-based design earthquake loads for single-degree-of-freedom inelastic structures. J. Struct. Eng. **137**, 456–467 (2011)

Moustafa, A., Mahmoud, S.: Damage assessment of adjacent buildings under earthquake loads. Eng. Struct. **61**, 153–165 (2014)

Nagarajaiah, S., Sun, X.: Base-isolated FCC building: impact response in Northridge earthquake. J. Struct. Eng. **127**, 1063–1075 (2001)

Newmark, N.: A method of computation for structural dynamics. J. Eng. Mech. Div ASCE **85**, 67–94 (1959)

NBC: National Building Code, Technical Standard of Building E.030. Earthquake Resistant Design. Ministry of Housing, Peru (2003)

Park, Y.J., Ang, A.H.S.: Mechanistic seismic damage model for reinforced concrete. J. Struct. Eng. **111**, 722–739 (1985)

Park, Y.J., Ang, A.H.S., Wen, Y.K.: Seismic damage analysis of reinforced concrete buildings. J. Struct. Eng. **111**, 740–757 (1985)

Park, Y.J., Ang, A.H.S., Wen, Y.K.: Damage-limiting aseismic design of buildings. Earthquake Spectra **3**, 1–26 (1987)

Polycarpou, P.C., Komodromos, P.: Earthquake-induced poundings of a seismically isolated building with adjacent structures. Eng. Struct. **32**, 1937–1951 (2010)

Powell, G.H., Allahabadi, R.: Seismic damage prediction by deterministic methods: concepts and procedures. Earthquake Eng. Struct. Dynam. **16**, 719–734 (1988)

Rajaram, C.R., Kumar, R.P.: Comparison of codal provisions on pounding between adjacent buildings. Int. J. Earth Sci. Eng. **5**, 72–82 (2012)

Ruangrassamee, A., Kawashima, K.: Relative displacement response spectra with pounding effect. Earthquake Eng. Struct. Dynam. **30**, 1511–1538 (2001)

Sołtysik, B., Jankowski, R.: Non-linear strain rate analysis of earthquake-induced pounding between steel buildings. Int. J. Earth Sci. Eng. **6**, 429–433 (2013)

UBC: Uniform Building Code. International Conference of Building Officials, USA (1997)

Valles R.E., Reinhorn A.M.: Evaluation, prevention and mitigation of pounding effects in building structures. Technical Report NCEER–97–0001: National Center for Earthquake Engineering Research. State University of New York at Buffalo, Buffalo, USA (1997)

Williams, M.S., Sexsmith, R.G.: Seismic damage indices for concrete structures: a state-of-the-art review. Earthquake Spectra **11**, 319–349 (1995)

Zembaty, Z.: Vibrations of bridge structure under kinematic wave excitations. J. Struct. Eng. **123**, 479–488 (1997)